Journal of the Physical Society of Japan **94**, 101005 (2025)
https://doi.org/10.7566/JPSJ.94.101005

Topological Photonic Integrated Circuits for Controlling Internal Degrees of Freedom of Light

Tomohiro Amemiya[1*], Sho Okada[2], XingXiang Wang[1], and Xiao Hu[1,3]

[1]*Department of Electrical and Electronic Engineering, Institute of Science Tokyo, Meguro, Tokyo 152-8552, Japan*
[2]*National Institute of Information and Communications Technology, Koganei, Tokyo 184-8795, Japan*
[3]*Shanghai University, Shanghai 200444, China*

(Received November 14, 2024; revised August 25, 2025; accepted August 26, 2025; published online September 30, 2025)

Topological photonics enables the systematic handling of internal degrees of freedom of light (optical spin and orbital angular momentum) in optical communications by introducing the concept of topology from mathematics into the field of photonics. This paper focuses on topological waveguides, which are the most important components in topological photonic systems, and explains the specific behavior caused by optical spins within waveguides.

1. Introduction

Topological electronic properties have attracted significant attention in recent years, with researchers anticipating the discovery of new physical phenomena associated with topologically protected surface states and the development of devices based on these states.[1–4)] Inspired by these advancements, research on topological photonics — where the topology of electronic systems is translated into photonic systems — has also gained momentum.[5,6)] A defining feature of topological photonic systems is the ability to create photonic structures with distinct mathematical properties by simultaneously controlling optical mode interactions within and between unit cells in nanoperiodic structures. This capability allows for greater flexibility in device design than photonic crystals, which primarily focus on inter-unit cell interactions,[7–10)] or metamaterials, which focus on intra-unit cell interactions.[11–18)]

One of the most well-known phenomena in topological photonic systems is the topological edge state, which occurs at the interface between two topologically distinct photonic structures and enables the propagation of light with specific spin and orbital angular momentum.[19,20)] From an engineering perspective, spin and orbital angular momentum of light can be represented as circular polarization and optical vortices, respectively, allowing different information to be conveyed in mutually orthogonal modes. For instance, circular polarization can have left- and right-handed modes, while optical vortices can encode information based on the number of helical turns. Thus, circular polarization and optical vortices are crucial for expanding optical transmission capacity.[21,22)] Topological photonics technology that enables the propagation and maintenance of these modes within optical circuits[23–32)] is expected to have a broad range of applications.

2. Topological Edge States of Light

Topology is a branch of mathematics that studies flexible shapes, such as rubber-like figures. In this field, a donut and a cup with a handle are considered the same shape, while a sphere and a torus are considered different because they cannot be deformed into one another, even when stretched or compressed. Here, the distinction between a sphere and a torus is based on the "number of holes", with shapes possessing a different number of holes regarded as distinct (mathematically expressed as having "different topologies").

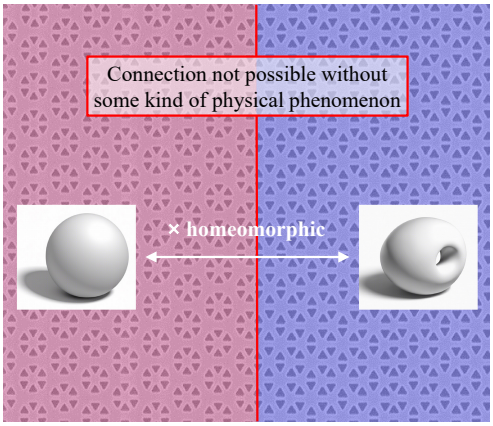

Fig. 1. (Color online) Conceptual framework of topological photonics.

Topological photonics applies these concepts to the study of light. To illustrate this idea, consider the example in Fig. 1, which shows two photonic structures with similar optical properties. Generally, placing two structures with similar optical properties side by side should not alter their behavior. However, if the two structures have different topologies, this assumption no longer holds. Just as a sphere cannot be continuously transformed into a torus, topologically distinct photonic structures cannot be continuously transformed into one another without passing through a unique physical state. This unique state, called the topological edge state, occurs at the interface between the two structures.

Light propagated by this topological edge state exhibits distinct characteristics in terms of spin and orbital angular momentum, such as circular polarization and optical vortex.

Properties with respect to optical spin: Light propagated by topological edge states exhibits a unique propagation direction for left- and right-circularly polarized light. Figure 2 shows the H_y component of light propagating through the adjacent interface when right-circularly polarized light is incident as a point source near the center of Fig. 1, where it propagates in only one direction. Left-circularly polarized light propagates in the opposite direction.

Properties with respect to optical orbital angular momentum: Light propagated by topological edge states generates localized vortices. Close examination of Fig. 2

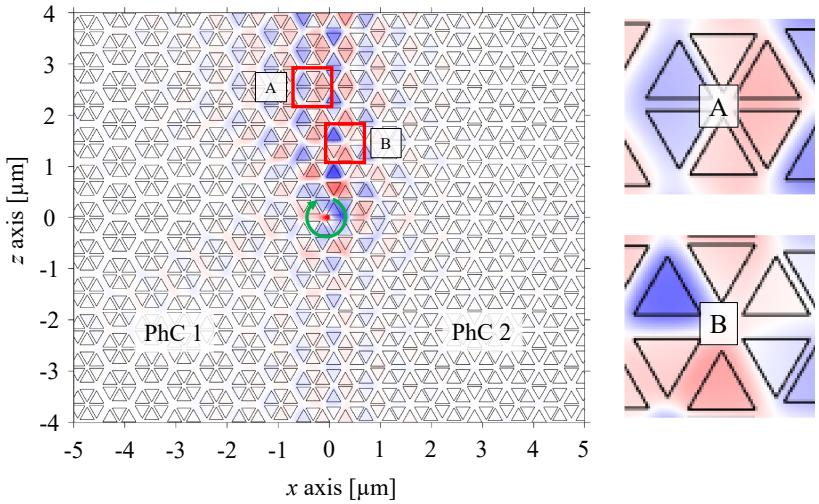

Fig. 2. (Color online) Characteristics of light propagated via topological edge states.

reveals that, while the energy of light propagating through adjacent interfaces flows in a specific overall direction, the light also forms local vortices at certain points. For example, in the areas shown by A and B in Fig. 2, the magnetic field distribution is a mixture of optical vortices with 2π and 4π.

3. Exploring Topological Concepts

These results suggest that unique physical phenomena occur at the adjacent interfaces of topologically distinct photonic structures. However, it is important to determine how to differentiate between phenomena arising from topologically distinct photonic structures.

Within photonic structures, arranging fine features smaller than the wavelength in a periodic manner allows for various manipulations of light due to the interaction between light and matter within the structure. Here, the photonic band is a key index that determines optical properties. It summarizes the dispersion relations of the electromagnetic wave modes in the target structure and is crucial for distinguishing between topologically distinct phenomena. For instance, certain photonic structures with a $\mathbb{Z}2$ topology (indicating two types of topological phases) allow for analysis by examining the behavior of electromagnetic modes near the band gap edge, particularly around the Γ point.[33,34]

To examine this aspect, we provide a specific experimental example. Figure 3 shows a scanning electron microscope image of the element used for evaluation. In this study, we employed a structure in which triangular nanoholes with C_{6v} symmetry were arranged in a honeycomb lattice on a silicon-on-insulator (SOI) substrate with a silicon film thickness of 220 nm. This structure has been mathematically proven to express a $\mathbb{Z}2$ topology, modulated by the distance R from the center of the honeycomb lattice to the center of each nanohole and the length L of one side of the nanohole.[33] The device was fabricated by applying ZEP520A to an SOI substrate, followed by electron beam exposure with proximity effect correction to form the device pattern. The silicon layer was then etched using inductively coupled reactive ion etching with SF_6–C_4F_8 mixture gas, using ZEP520A as the mask.

In this study, we developed a photonic band microscope based on hyperspectral Fourier imaging spectroscopy to measure the photonic band of the fabricated structure at high

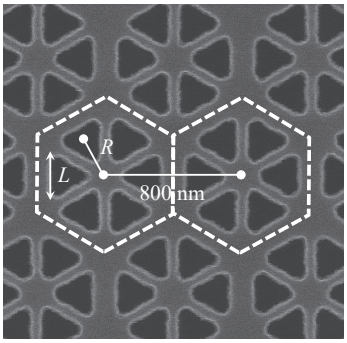

Fig. 3. Scanning electron microscope image of a photonic structure with Z2 topology.

speed and over a wide-angle range, as shown in Fig. 4.[35] Light from a broadband white light source (Bentham WLS100, wavelength range: 300–2500 nm) was incident to the device through a ×60 objective lens (NA 0.9, Olympus Plan Fluorite Objective, UPLFLN60X). The Fourier image of light scattered from the element was captured with an infrared camera through a 4f optical system. A tunable filter (CRI, VariSpec LNIR, bandwidth: 6 nm) positioned in front of the infrared camera allowed for the acquisition of diffraction patterns at wavelengths ranging from 850 to 1800 nm.

The procedure for obtaining a photonic band using this configuration is as follows. In this study, we utilized software to fully automate the entire sequence, prioritizing the system's high speed and versatility. (i) First, a Fourier image of the scattered light from the device was captured while varying the central wavelength of the tunable filter. (ii) Next, the intensity along a specified path was measured for each Fourier image, which was then converted into an intensity distribution of a specific energy in reciprocal lattice space. (iii) Finally, this process was repeated for all wavelengths to construct the photonic band. Here the energy and momentum resolutions were given by the bandwidth of the tunable filter and the momentum resolution was determined by the pixels of the infrared camera.

Figure 5 presents the measurement results for two representative photonic structures with different topologies, where (R, L) = (230 nm, 250 nm) and (290 nm, 250 nm), with

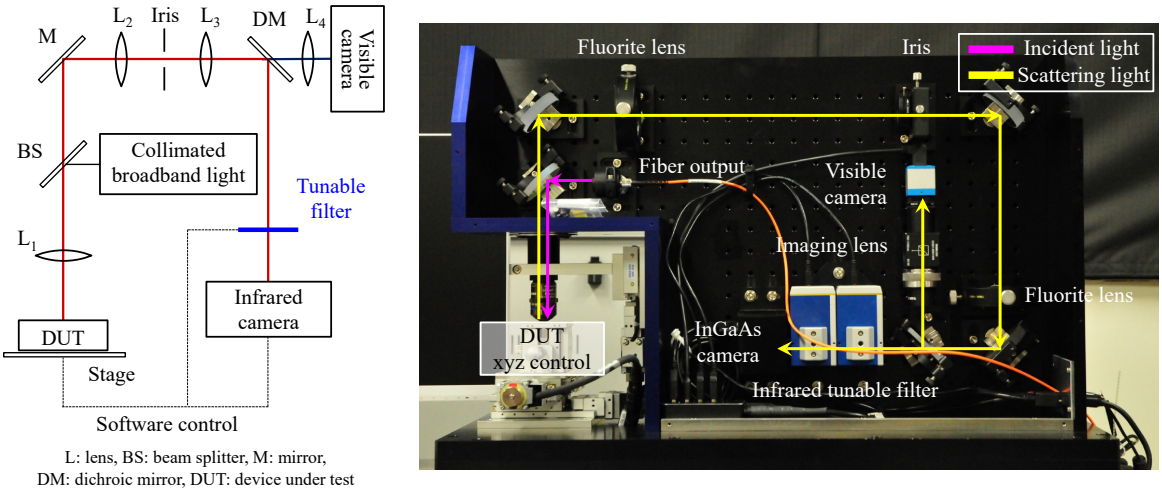

Fig. 4. (Color online) Hyperspectral Fourier imaging spectroscopy for photonic band measurement. This figure is taken from Ref. 35. © 2022 Optica Publishing Group under the terms of the Optica Open Access Publishing Agreement.

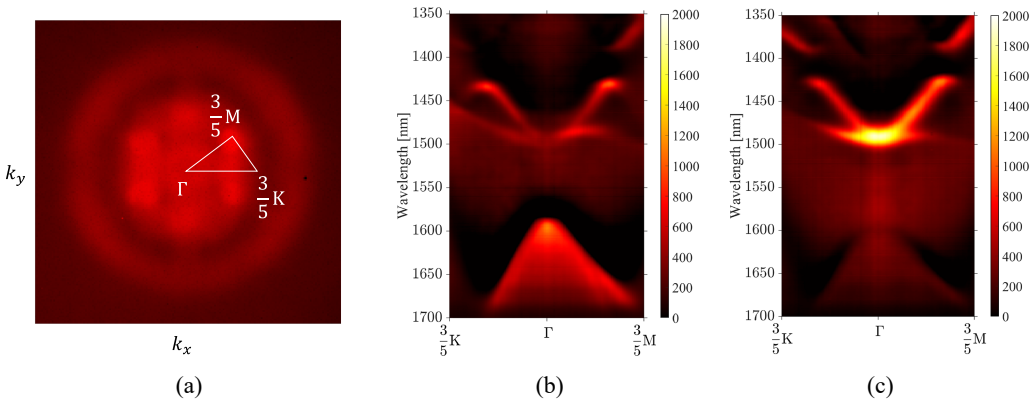

Fig. 5. (Color online) (a) Fourier image of scattered light from a photonic structure. (b, c) Measurement results of bands in two typical topologically distinct photonic structures. This figure is taken from Ref. 35. © 2022 Optica Publishing Group under the terms of the Optica Open Access Publishing Agreement.

a fixed lattice spacing of 800 nm. Figure 5(a) shows the Fourier image of the scattered light from the device, where distinct changes due to the photonic band were observed at each wavelength. Figures 5(b) and 5(c) display the reconstructed photonic bands, with measurements taken along the Γ–K–M path, corresponding to the honeycomb lattice in Fig. 5(a). The results indicate a band gap near 1.5 μm, and the intensity at the upper and lower band gap edges near the Γ point is inverted.

The results of this experiment indicate that the electromagnetic modes of p- and d-waves are inverted at the Γ point. This inversion occurs because the reflection intensity of the electromagnetic mode of d-waves is weaker than that of p-waves (d-waves are generally located below the light line, and scattering is suppressed compared to p-waves), enabling observation of the phenomenon of "different topologies".[33,34]

4. Optical Spin Propagated by Topological Edge States

As previously discussed, light propagated by topological edge states exhibits distinctive properties concerning spin and orbital angular momentum. In this section, we focus on spin (circular polarization) and demonstrate that placing two topologically distinct photonic structures adjacent to each other induces unique behavior in the light propagating through the interface.

Figure 6 shows a scanning electron microscope image of the device used in this study. Here, two topologically different photonic structures are in contact at a zig-zag interface, creating a topological waveguide via the edge state at the interface. Topological converters[36] are positioned on both sides of the topological waveguide to achieve efficient coupling with the silicon waveguide. Figure 7 shows experimental setup. In this experiment, TE-mode light from a tunable laser was incident to the device through a polarization-maintaining fiber, and propagation characteristics of the topological waveguide were evaluated using a spectrum analyzer and power monitor. An infrared camera is positioned at the top of the device via a $\lambda/4$ waveplate and a linear polarizer. By rotating the polarizer, it is possible to observe scattered light from the device for either left- or right-handed circular polarization.

Figure 8(a) illustrates the wavelength dependence of the propagation characteristics of this topological waveguide. Within the photonic band gap (1530–1610 nm in this device), low-loss propagation (∼0.1 dB/cell) is achieved, and a reduction in propagation loss due to spin–spin scattering is observed near the center of the band gap.

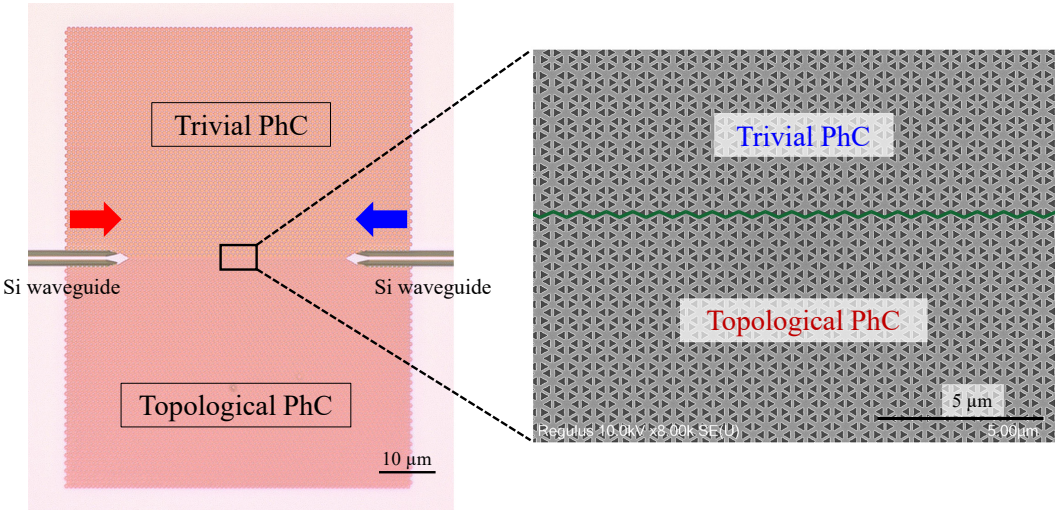

Fig. 6. (Color online) Optical microscope image and scanning electron microscope image of topological waveguide composed of topological edge states.

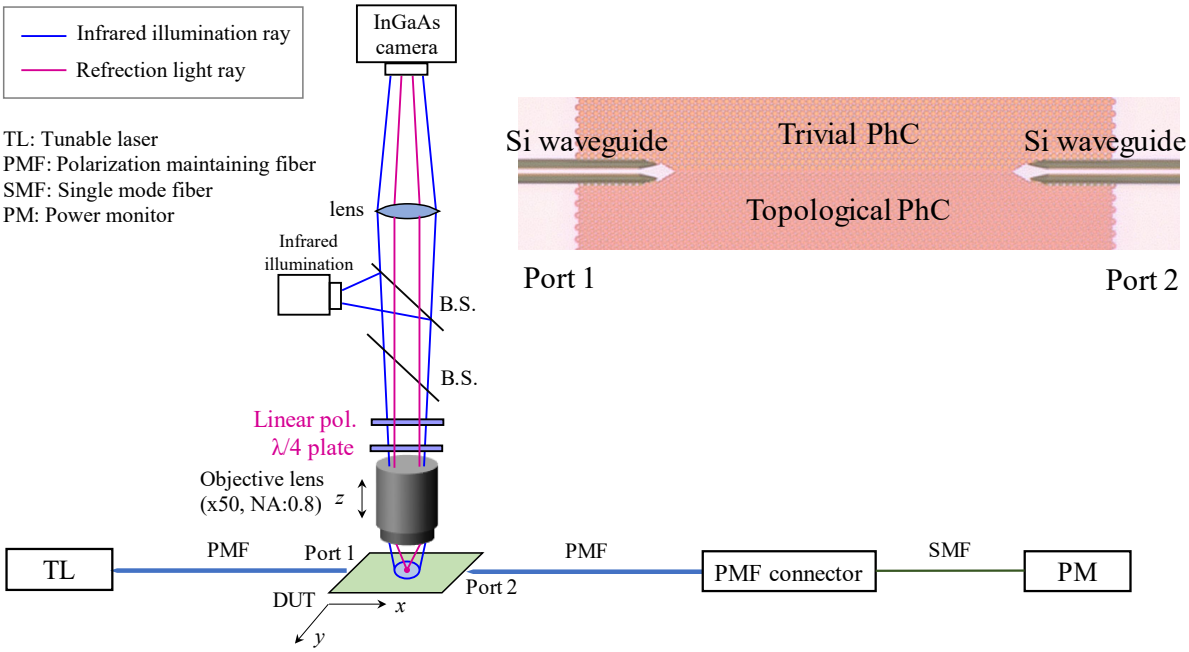

Fig. 7. (Color online) Measurement of optical spin propagation in a topological waveguide under horizontal incidence.

The aforementioned results indicate the generation of a topological edge state at the interface between the two photonic structures, facilitating light propagation. A polarizer and $\lambda/4$ waveplate were placed above the device through an objective lens to estimate the degree of circular polarization by observing the scattered light intensity with an infrared camera. Figures 8(b) and 8(c) present these results. The change in intensity with the polarizer angle exhibits a figure-eight pattern, confirming that the propagating light is fully circularly polarized. Furthermore, the direction of circular polarization (left or right) is uniquely determined by the direction of light propagation through the topological waveguide, suggesting the emergence of optical spin properties as discussed in Sect. 2.

Next, as shown in Fig. 9, the characteristics of optical spin were observed with vertically incident light on the topological waveguide. In this experiment, light from a tunable laser was passed through a polarization-maintaining fiber and a collimating lens, followed by a polarizer and $\lambda/4$ waveplate to produce left and right circularly polarized plane waves. The light was then directed onto the device from above using an objective lens (Olympus LCPLFLN20XLCD: NA 0.9). The vertical coupling efficiency of the device was enhanced by removing triangular nanoholes from a specific lattice area near the topological waveguide, hereafter referred to as the "defect structure". The defect structure consists of a honeycomb lattice filled with a high-refractive-index dielectric, forming a cavity that tightly confines vertically incident light. Simultaneously, the topological edge state surrounding the defect is disrupted, enabling highly efficient coupling of the confined light to the topological waveguide.[37,38] The light propagating through the topological waveguide was directed to a polarization-maintaining fiber, and its propagation characteristics were evaluated using a spectrum analyzer and power monitor. An in-line polarizer was inserted into the polarization-maintaining fiber on the output side to eliminate stray light.

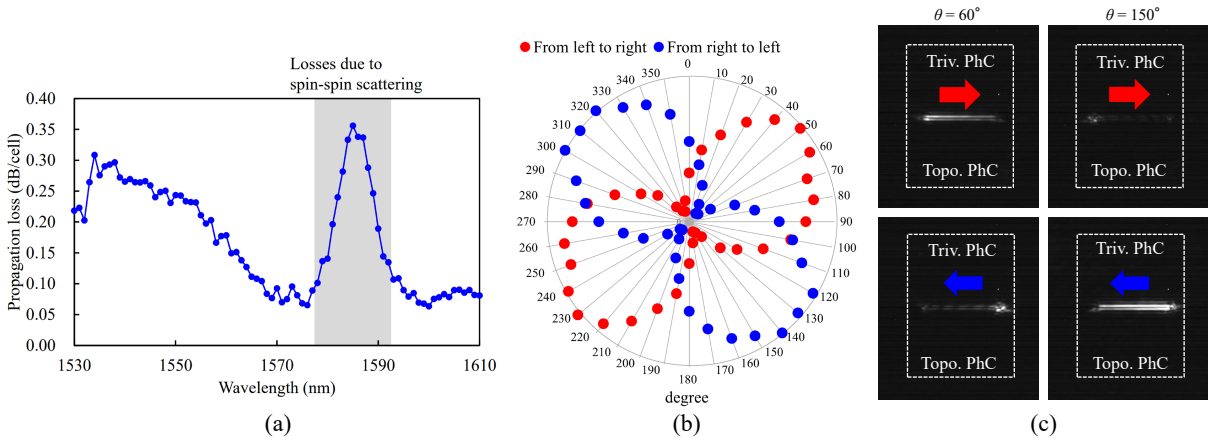

Fig. 8. (Color online) (a) Propagation loss of the topological waveguide. (b, c) Degree of circular polarization of propagating light in the topological waveguide.

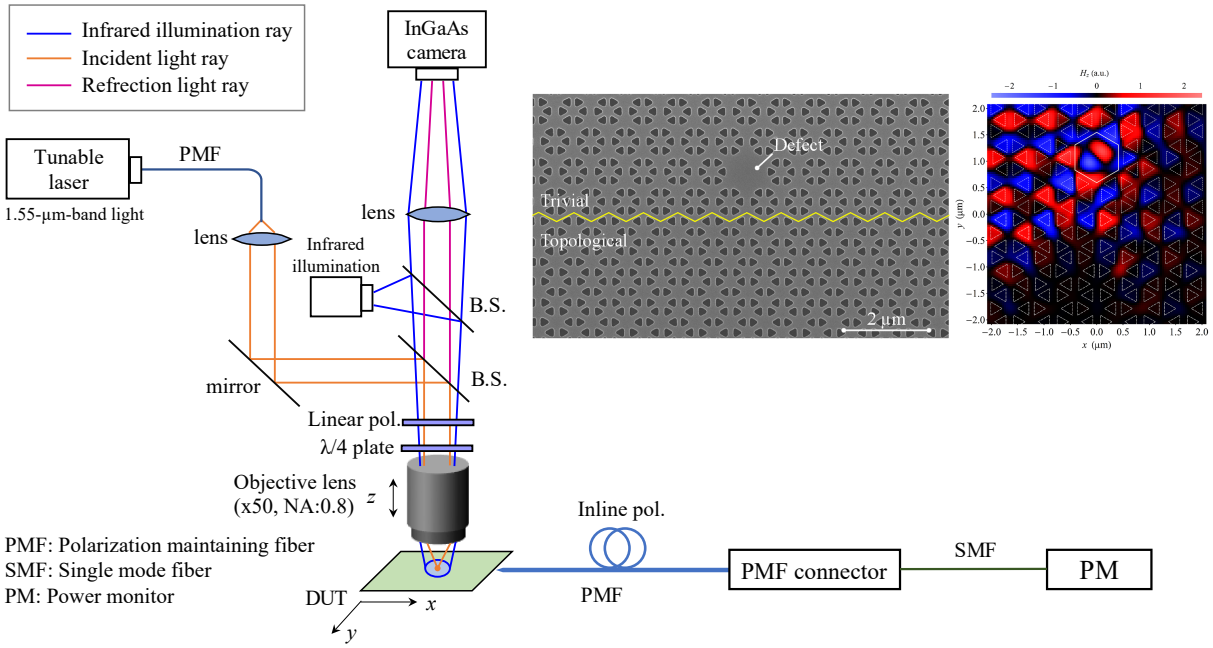

Fig. 9. (Color online) Measurement of optical spin propagation in a topological waveguide under vertical incidence. This figure is taken from Ref. 38.

Figure 10 shows the wavelength dependence of the output intensity from each port when left and right circularly polarized light are incident on the device. Figure 10(a) presents the output intensity from the same port for left and right circularly polarized light, demonstrating a unique characteristic of the topological edge state: specific circularly polarized light propagates uniquely, with right circularly polarized light primarily output to port 1 and left circularly polarized light primarily output to port 2. The output intensity ratio between the two ports reached up to approximately 20 dB within the defect structure's operating wavelength range (1550–1580 nm). Figure 10(b) illustrates the output intensity from the port where each circular polarization is dominant. The propagation characteristics are nearly identical for both circular polarizations in each direction, strongly reflecting the optical spin properties of the topological edge state.

5. Conclusions

In this study, we described the topological edge state that arises at the interface between two topologically distinct photonic structures. As previously mentioned, light propagated by the topological edge state exhibits a unique phenomenon where the propagation direction is determined specifically for left- and right-circular polarization. By treating left- and right-circularly polarized light as the up- and down-spin of a photon, respectively, this phenomenon becomes analogous to the spin-momentum locking observed in topological insulators. Topological photonics is an interdisciplinary field that integrates mathematics, optics, and solid-state physics, emphasizing the approach of "examining phenomena from various perspectives". Discussing phenomena from a multifaceted, cross-disciplinary viewpoint, rather than through simple observation, allows for a more comprehensive understanding of their characteristics.

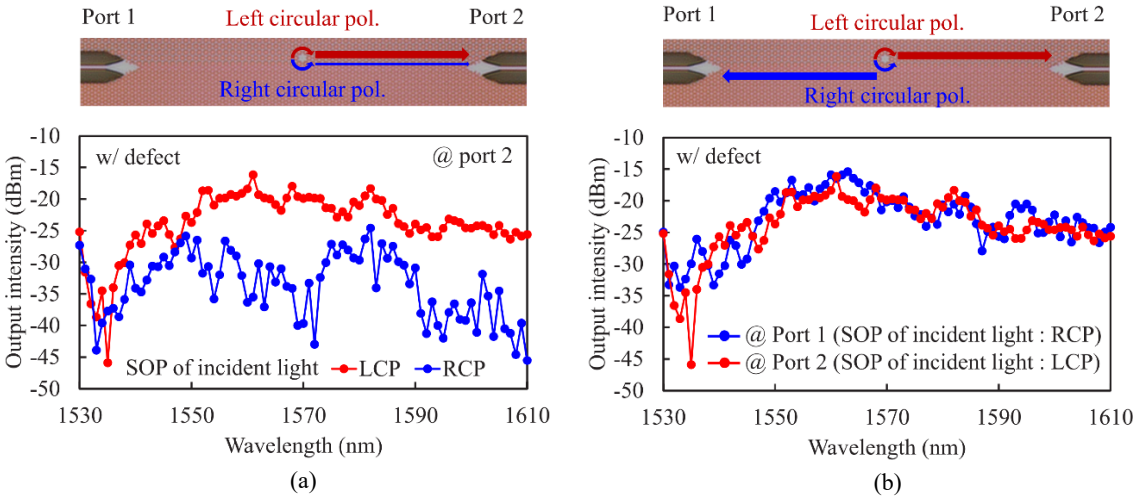

Fig. 10. (Color online) Wavelength-dependent output intensity for each port both left- and right-circularly polarized light incident. (a) Output intensity from the same port for left- and right-circularly polarized light. (b) Output intensity from a different port for left- and right-circularly polarized light. This figure is taken from Ref. 38. © 2023 Optica Publishing Group under the terms of the Optica Open Access Publishing Agreement.

Acknowledgment This work was partially supported by JST CREST (JPMJCR24R1), JST ASPIRE (23837157), JSPS KAKENHI (25H00734).

*amemiya.t.ab@m.titech.ac.jp

1) M. Z. Hasan and C. L. Kane, Rev. Mod. Phys. **82**, 3045 (2010).
2) X.-L. Qi and S.-C. Zhang, Rev. Mod. Phys. **83**, 1057 (2011).
3) D. Xiao, M.-C. Chang, and Q. Niu, Rev. Mod. Phys. **82**, 1959 (2010).
4) H. Weng, R. Yu, X. Hu, X. Dai, and Z. Fang, Adv. Phys. **64**, 227 (2015).
5) Z. Wang, Y. Chong, J. D. Joannopoulos, and M. Soljacic, Nature **461**, 772 (2009).
6) T. Ozawa, H. M. Price, A. Amo, N. Goldman, M. Hafezi, L. Lu, M. C. Rechtsman, D. Schuster, J. Simon, O. Zilberberg, and I. Carusotto, Rev. Mod. Phys. **91**, 015006 (2019).
7) J. Joannopoulos, P. Villeneuve, and S. Fan, Nature **386**, 143 (1997).
8) T. Baba, Nat. Photonics **2**, 465 (2008).
9) K. Yasumoto, *Electromagnetic Theory and Applications for Photonic Crystals* (CRC Press, New York, 2018).
10) M. A. Butt, S. N. Khonica, and N. L. Kazanskiy, Opt. Laser Technol. **142**, 107265 (2021).
11) J. B. Pendry, A. J. Holden, D. J. Robbins, and W. J. Stewart, IEEE Trans. Microwave Theory Tech. **47**, 2075 (1999).
12) R. A. Shelby, D. R. Smith, and S. Schultz, Science **292**, 77 (2001).
13) N. I. Zheludev and Y. S. Kivshar, Nat. Mater. **11**, 917 (2012).
14) I. Staude and J. Schilling, Nat. Photonics **11**, 274 (2017).
15) T. Amemiya, A. Ishikawa, T. Kanazawa, J. H. Kang, N. Nishiyama, Y. Miyamoto, T. Tanaka, and S. Arai, Sci. Rep. **5**, 8985 (2015).
16) T. Amemiya, S. Yamasaki, M. Tanaka, H. Kagami, K. Masuda, N. Nishiyama, and S. Arai, Opt. Express **27**, 15007 (2019).
17) P. Yu, L. V. Besteiro, Y. Huang, J. Wu, L. Fu, H. H. Tan, C. Jagadish, G. P. Wiederrecht, A. O. Govorov, and Z. Wang, Adv. Opt. Mater. **7**, 1800995 (2019).
18) Y. Honda, Y. Shoji, and T. Amemiya, Opt. Lett. **49**, 5811 (2024).
19) M. Kim, Y. Kim, and J. Rho, New J. Phys. **22**, 113022 (2020).
20) N. Parappurath, F. Alpeggiani, L. Kuipers, and E. Verhagen, Sci. Adv. **6**, eaaw4137 (2020).
21) H. Huang, G. Xie, Y. Yan, N. Ahmed, Y. Ren, Y. Yue, D. Rogawski, M. J. Willner, B. I. Erkmen, K. M. Birnbaum, S. J. Dolinar, M. P. J. Lavery, M. J. Padgett, M. Tur, and A. E. Willner, Opt. Lett. **39**, 197 (2014).
22) T. Amemiya, T. Yoshida, Y. Atsumi, N. Nishiyama, Y. Miyamoto, and S. Arai, Proc. OFC, 2019, M1C.7.
23) T. Shindo, T. Okumura, H. Ito, T. Koguchi, D. Takahashi, Y. Atsumi, J. Kang, R. Osabe, T. Amemiya, N. Nishiyama, and S. Arai, IEEE J. Sel. Top. Quantum Electron. **17**, 1175 (2011).
24) J. Kang, Y. Atsumi, M. Oda, T. Amemiya, N. Nishiyama, and S. Arai, Jpn. J. Appl. Phys. **51**, 120203 (2012).
25) J. Kang, Y. Atsumi, Y. Hayashi, J. Suzuki, Y. Kuno, T. Amemiya, N. Nishiyama, and S. Arai, Appl. Phys. Express **7**, 032202 (2014).
26) D. Inoue, T. Hiratani, Y. Atsuji, T. Tomiyasu, T. Amemiya, N. Nishiyama, and S. Arai, IEEE J. Sel. Top. Quantum Electron. **21**, 1502907 (2015).
27) Z. Gu, T. Amemiya, A. Ishikawa, T. Hiratani, J. Suzuki, N. Nishiyama, T. Tanaka, and S. Arai, Opt. Express **23**, 22394 (2015).
28) Y. Hayashi, J. Suzuki, S. Inoue, S. Hasan, Y. Kuno, K. Itoh, T. Amemiya, N. Nishiyama, and S. Arai, Jpn. J. Appl. Phys. **55**, 082701 (2016).
29) T. Hiratani, D. Inoue, T. Tomiyasu, K. Fukuda, T. Amemiya, N. Nishiyama, and S. Arai, IEEE J. Sel. Top. Quantum Electron. **23**, 3700108 (2017).
30) T. Tomiyasu, D. Inoue, T. Hiratani, K. Fukuda, N. Nakamura, T. Uryu, T. Amemiya, N. Nishiyama, and S. Arai, Appl. Phys. Express **11**, 012704 (2018).
31) Z. Gu, D. Inoue, T. Amemiya, N. Nishiyama, and S. Arai, Appl. Phys. Express **11**, 022102 (2018).
32) Y. Wang, K. Nagasaka, T. Mitarai, Y. Ohiso, T. Amemiya, and N. Nishiyama, Jpn. J. Appl. Phys. **59**, 052004 (2020).
33) L.-H. Wu and X. Hu, Phys. Rev. Lett. **114**, 223901 (2015).
34) S. Okada, T. Amemiya, H. Kagami, Y. Wang, N. Nishiyama, and X. Hu, J. Opt. Soc. Am. B **39**, 2464 (2022).
35) T. Amemiya, S. Okada, H. Kagami, N. Nishiyama, Y. Yao, K. Sakoda, and X. Hu, Opt. Lett. **47**, 2430 (2022).
36) H. Kagami, T. Amemiya, S. Okada, N. Nishiyama, and X. Hu, Opt. Express **28**, 33619 (2020).
37) H. Kagami, T. Amemiya, S. Okada, N. Nishiyama, and X. Hu, Opt. Express **29**, 32755 (2021).
38) S. Okada, H. Kagami, N. Nishiyama, X. Hu, and T. Amemiya, Opt. Express **31**, 35218 (2023).